Computational Statistics & Data Analysis
January 2015, Volume 81, Pages 24-37
http://dx.doi.org/10.1016/j.csda.2014.07.010

Modeling process asymmetries with Laplace moving average

Nicolas Raillard[a, *], Marc Prevosto[a], Pierre Ailliot[b]

[a] Laboratoire Comportement des Structures en Mer, IFREMER, France
[b] Laboratoire de Mathématiques de Bretagne Atlantique, Université de Bretagne Occidentale, Brest, France

*: Corresponding author : Nicolas Raillard, email address : nicolas.raillard@gmail.com
marc.prevosto@ifremer.fr ; pierre.ailliot@univ-brest.fr

Abstract:

Many records in environmental science exhibit asymmetries: for example in shallow water and with variable bathymetry, the sea wave time series shows front–back asymmetries and different shapes for crests and troughs. In such situation, numerical models are available but their computational cost and complexity are high. A stochastic process aimed at modeling such asymmetries has recently been proposed, the Laplace moving average process, which consists in applying a linear filter on a non-Gaussian noise built using the generalized Laplace distribution. The objective is to propose a new non-parametric estimator for the kernel involved in the definition of this process. Results based on a comprehensive numerical study will be shown in order to evaluate the performances of the proposed method.

Keywords: Laplace moving average ; Non-linear time series ; FIR estimation ; Splines ; High-order spectrum ; Asymmetries

1. Introduction

Marine coastal systems are subject to loadings due to sea waves, and long time series of the loadings are often needed to carry out studies of the performances of the system or to assess its extremal behavior. During its lifetime, this system is likely to encounter various sea states, and thus one needs to be able to simulate long and numerous series with realistic characteristics. Many such systems are located near the shore, in shallow water and with variable bathymetry. In this context, the waves are known to be non-linear, and show high asymmetries. Two kinds of asymmetries can arise in this context: the top–bottom (vertical) asymmetry and the front–back (horizontal) asymmetry. The first one describes the different behavior of troughs compared to crests with the peaks being generally sharper compared to the bottom. The second kind of asymmetry is linked to the time irreversibility: for example, the front steepness of crests is higher than the back one. Many other situations in natural and social sciences lead to similar asymmetries.

The aforementioned criteria are known to be impossible to reproduce with Gaussian processes, and models with such asymmetries must be developed. Recently, such a model has been proposed (Podgórski and Wegener, 2010 and Aberg and Podgórski, 2011), along with a description of some of its properties (Galtier et al., 2010 and Galtier, 2011) and an estimation procedure of some of its characteristics (Podgórski and Wegener, 2011). The model is a linear filter of a non-Gaussian noise built using the generalized Laplace distribution. The goal of the study is thus to propose a new method for estimating the kernel, which is an unknown function that rules the behavior of the process, and then to study the behavior of this estimator both on simulated and real data.

The paper is organized as follows. The first section introduces the model and some of its characteristics, and in particular the high-order spectrum properties that is used in the estimation procedure which is discussed in the second section. In a third section, we present a simulation study to assess the performances of the new estimation procedure. An application on a real dataset is carried out in the fourth section. Conclusions and key findings are given in Section 5.

2. Description of the LMA model

2.1. Model construction

The construction of the process is based on a non-Gaussian noise, itself based on a non-Gaussian distribution, intended to be flexible and capable to handle heavy tails and distributional asymmetries, the *Generalized Asymmetric Laplace distribution*.

Definition 1 (Generalized Asymmetric Laplace distribution). *The following characteristic function defines a distribution called 'Generalized Asymmetric Laplace distribution' ($\mathcal{GAL}$):*

$$\Phi(u) = e^{i\delta u}\left(1 - i\mu u + \frac{\sigma^2 u^2}{2}\right)^{-1/\nu},$$

where $\delta,\ \mu \in \mathbb{R}$, $\nu > 0$ and $\sigma > 0$. The cases $\nu = 1$ and $\mu = 0$ are referred to as the asymmetric Laplace distribution and the generalized symmetric Laplace, respectively.

This distribution has finite moments of any order and in particular if $Y \sim \mathcal{GAL}(\delta, \mu, \sigma, \nu)$, then

$$\begin{array}{cc} \mathbb{E}Y = \frac{\mu}{\nu} + \delta & \mathbb{V}Y = \frac{\mu^2+\sigma^2}{\nu} \\ s(Y) = \mu\sqrt{\nu}\frac{2\mu^2+3\sigma^2}{(\mu^2+\sigma^2)^{3/2}} & \kappa_e(Y) = 3\nu\left(2 - \frac{\sigma^4}{(\mu^2+\sigma^2)^2}\right) \end{array},$$

where s denotes the skewness and κ_e the excess kurtosis. This distribution shows great flexibly, with various shapes for the density function as it can be seen on Figure 1. This figure shows 8 densities all such that the mean is equal to 0 and variance to 1. The left plot contains symmetric distributions, while the right plot shows asymmetric densities.

Thanks to the infinite divisibility property of the $\mathcal{GAL}$ distribution, one can construct also a Levy process, with stationary and independent increments from a $\mathcal{GAL}$, called a Laplace motion (see [5]):

Definition 2 (Laplace motion). *A Laplace motion Γ is defined by the following conditions:*

- *it starts at the origin (i.e. $\Gamma(0) = 0$);*
- *its increments are stationary and independent;*
- *the increments by the time unit ν have a zeros mean asymmetric Laplace distribution.*

This process is also referred as the Variance-Gamma process, see [6].

Once we have such a process constructed, it becomes possible to define the process that will be intensively used in the sequel, namely a convolution of a Laplace motion with some function. This leads to a stationary linear process which is linear but non-Gaussian, with the ability to produce asymmetries, see [1] for more details.

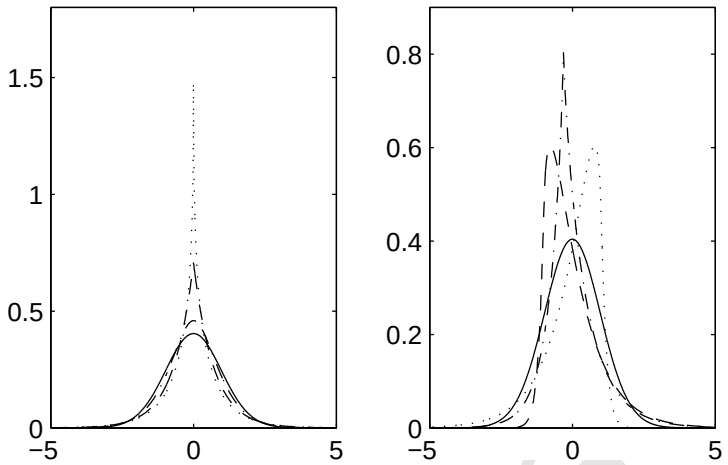

Figure 1: Densities of GAL distributions

Definition 3 (Laplace moving average). *Let* Γ *be a Laplace motion with zero mean and* f *a function with values in* $\mathbb{R}$*, named* kernel *such that both* $\int_{\mathbb{R}} f$ *and* $\int_{\mathbb{R}} f^2$ *are finite. Then,*

$$X_t = \int_{\mathbb{R}} f(t-x)d\Gamma(x) \tag{1}$$

defines a stationary stochastic process on $\mathbb{R}$*, called a* Laplace moving average ($\mathcal{LMA}$)*. Such a process will be referred as* $\mathcal{LMA}(\mu, \sigma, \nu; f)$*.*

2.2. Process properties

A lot of properties can be derived for this process, whose proofs can be found in the already cited articles. We will here only recall the properties that will be useful from a modeling point of view. We will describe both the margins and the second order structure, and will also see that a same second order structure can correspond to infinitely many different processes, depending on some characteristic of the kernel, namely the phase of the transfer function. We will then show that this phase can be identified using higher order structure.

2.2.1. Marginal distribution

According to [1] and [2], the $\mathcal{LMA}$ process is based on $\mathcal{GAL}$ distribution, and one can compute the characteristic function of the marginal distribution for such process:

$$\phi_{X_t}(u) = e^{-iu\mu/\nu \int f} \times \exp\left\{-\frac{1}{\nu}\int_{\mathbb{R}} \log\left(1 - iu\mu f(x) + \frac{\sigma^2 u^2 f^2(x)}{2}\right) dx\right\}.$$

In particular we get

$$\mathbb{E}X_t = 0; \tag{2}$$

$$\mathbb{V}X_t = \frac{\sigma^2+\mu^2}{\nu}\int_{\mathbb{R}} f^2; \tag{3}$$

$$s(X_t) = \frac{\mu}{\sqrt{\nu}}\frac{2\mu^2+3\sigma^2}{(\mu^2+\sigma^2)^{3/2}}\frac{\int_{\mathbb{R}} f^3}{(\int_{\mathbb{R}} f^2)^{3/2}}; \tag{4}$$

$$\kappa_e(X_t) = 3\nu\left(2-\frac{\sigma^4}{(\mu^2+\sigma^2)^2}\right)\frac{\int_R f^4}{(\int_{\mathbb{R}} f^2)^2}. \tag{5}$$

The scale of the kernel is still non identifiable, since any multiplicative constant on the kernel will lead to the same process, just by allowing σ and μ to change the opposite way. So, we impose in the sequel the constraint $\int_{\mathbb{R}} f^2 = 1$, to stay consistent with previous studies.

Another important property of this process is stated below.

Property 1. *Let X_t be a $\mathcal{LMA}(\mu,\sigma,\nu;f)$, and denote s and κ_e its skewness and excess kurtosis, respectively. Then $\kappa_e \geq 0$ and if $\kappa_e > 0$, then*

$$\frac{s(X_t)^2}{\kappa_e(X_t)} \leq \frac{2}{3}\frac{(\int f^3)^2}{\int f^4 \int f^2}. \tag{6}$$

Equation 6 can be interpreted as follows: for a given skewness, the distribution can not be too light tailed (low κ_e). In every case, the tail is heavier or comparable to the one of a normal distribution, and the excess kurtosis depends on the skewness. For a Generalized Laplace distribution, the equation (6) reads $\frac{s^2}{\kappa} \leq \frac{2}{3}$ and this is also the upper bound for $\frac{s^2}{\kappa_e}$ for a $\mathcal{LMA}$, since thanks to the Cauchy-Schwarz inequality, we have for any f, $\frac{(\int f^3)^2}{\int f^4 \int f^2} \leq 1$. It means that for a $\mathcal{LMA}$, the space of values of skewness and kurtosis that can be described is smaller than for a Generalized Laplace distribution.

2.2.2. Second order structure

The usual tool for time series modeling is the second order structure, since for a Gaussian process, this structure completely defines the process. We will see that it is no more the case with $\mathcal{LMA}$ processes. For instance, the covariance function r of X_t is given by

$$r(\tau) = \frac{\sigma^2+\mu^2}{\nu}\int_{\mathbb{R}} f(x-\tau)f(x)dx = \frac{\sigma^2+\mu^2}{\nu}(f * \tilde{f})(\tau),$$

where $\tilde{f}(x) = f(-x)$ and $*$ is the convolution operator. The power spectrum S of X_t is given by

$$S(\omega) = \frac{\sigma^2+\mu^2}{\nu}|\mathcal{F}(f)(\omega)|^2, \tag{7}$$

where $F = \mathcal{F}(f)$ denotes the Fourier transform of f and will be referred as *transfer function* in the sequel.

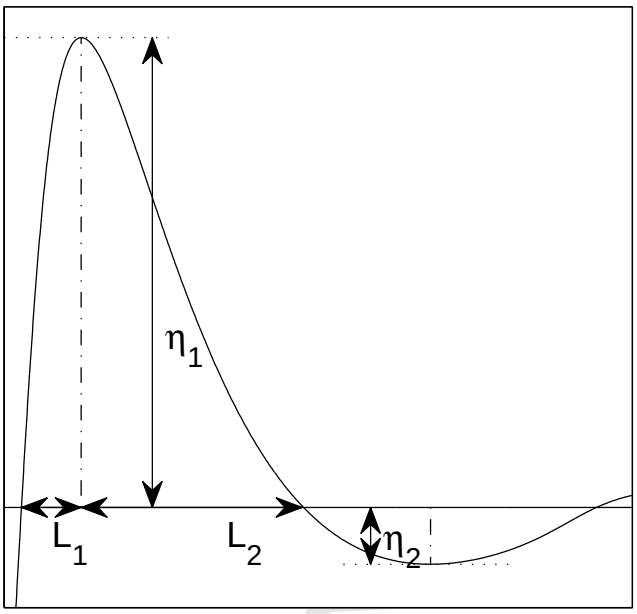

Figure 2: Asymmetry criterion

2.3. Influence of the kernel

As it can be seen from the previous equations, only the magnitude of the transfer function has an influence on the second order structure of the process. It means that there is still infinitely many transfer functions that lead to the same covariance for the process, but that may lead to processes with different properties. We study hereafter how the phase of the transfer function does influence the dynamical properties of the process using simulations.

Following [7], we looked at some characteristics of the record that will help us in quantifying the asymmetries of the data. Figure 2 represents an asymmetric wave and the asymmetry criteria discussed hereafter:

- $\delta_{\text{up}}^{\text{Crest}} = \frac{\eta_1}{L_1}$, the crest front steepness;
- $\delta_{\text{down}}^{\text{Crest}} = \frac{\eta_1}{L_2}$, the crest back steepness;
- $\delta_{\text{up}}^{\text{Trough}}$ and $\delta_{\text{down}}^{\text{Trough}}$ can also be defined for the troughs in a similar manner.

The estimation of those characteristics from observations is straightforward, using zero crossings to define the waves. A classical criterion to measure the steepness of the front face of waves is the asymmetry criterion, which is defined as the skewness of the derivative of the process, but that can be computed as the skewness of the Hilbert transform of the process (see e.g [8] and [9]). This criterion is defined A hereafter.

In order to study those quantities, we simulated two $\mathcal{LMA}$ processes with the same parameters for the Laplace noise and the same second order structure, i.e same spectrum or autocorrelation

Process	$\delta_{\text{up}}^{\text{Crest}}$	$\delta_{\text{down}}^{\text{Crest}}$	$\delta_{\text{up}}^{\text{Trough}}$	$\delta_{\text{down}}^{\text{Trough}}$	A
Non-symmetric kernel	0.41	0.56	0.33	0.46	-0.21
Symmetric kernel	0.55	0.55	0.33	0.33	0.00
Gaussian process	0.45	0.45	0.45	0.45	0.00

Table 1: Estimation of the asymmetry criteria from 1000 independent replicates of process with length 2^{22} and same second order structure and same parameters for the noise: $\lambda = 0,\ \psi = 1,\ \xi = 0.2,\ \zeta = 0.6$

function. The two kernels are depicted in the upper left plot of Figure 3. The non-symmetric kernel is defined by

$$f_1(x) = x^2 e^{-x} \mathbb{1}_{\mathbb{R}^+}(x) \tag{8}$$

and the symmetric one is defined by

$$f_2(x) = \mathcal{F}^{-1}\left[|\mathcal{F}(f_1)|\right]. \tag{9}$$

Both kernels have Fourier transforms with the same magnitude.

Examples of trajectories that can be obtained with those kernels are shown in Figure 3, in the upper right plot. The trajectories seem obviously to differ although the two processes share the same autocorrelation function, as depicted in the same figure, bottom left plot.

As it can be seen from Figure 3 and Table 1, the kernel has a great influence on the tilting of the trajectories. For example, the symmetric kernel will not be able to produce any front-back asymmetries since δ_{up} and δ_{down} are equal, although the crests and troughs can behave differently. It is also noticeable that the asymmetry criterion A differs clearly depending on the process.

We have seen that $\mathcal{LMA}$ processes with the same spectrum and same noise parameters will exhibit completely different behaviors. This is the reason why we will have to focus on higher order spectrum to explain such different dynamical properties. This is analogous to the marginal properties: a Gaussian distribution is described by its first two moments, but a generalized asymmetric Laplace will need the first four moments; a Gaussian process is characterized completely by its autocorrelation function, and a $\mathcal{LMA}$ is obviously not, according to the results above.

2.4. High-order spectrum

To distinguish between two $\mathcal{LMA}$ with the same spectrum, we can look at the high order spectra. For sake of simplicity, we will introduce only the bispectrum, or third order spectrum, but generalization to higher order is straightforward. First of all, let us recall the expression of the third order cumulant function of a stationary stochastic process X_t:

$$C_3(\tau_1, \tau_2) = \mathbb{E}[X_t X_{t+\tau_1} X_{t+\tau_2}].$$

Its Fourier transform is referred as the third-order spectrum (or bispectrum):

$$S_3(\omega_1, \omega_2) = \mathcal{F}_{2\text{D}}[C_3](\omega_1, \omega_2), \tag{10}$$

where $\mathcal{F}_{2\text{D}}$ denotes the 2D Fourier transform. In the sequel, the subscript will be omitted to simplify the presentation.

In the next section, an empirical estimate of the bispectrum is needed. Discussing this in details would go beyond the scope of this study and the reader may refer to [10] or [11] for a

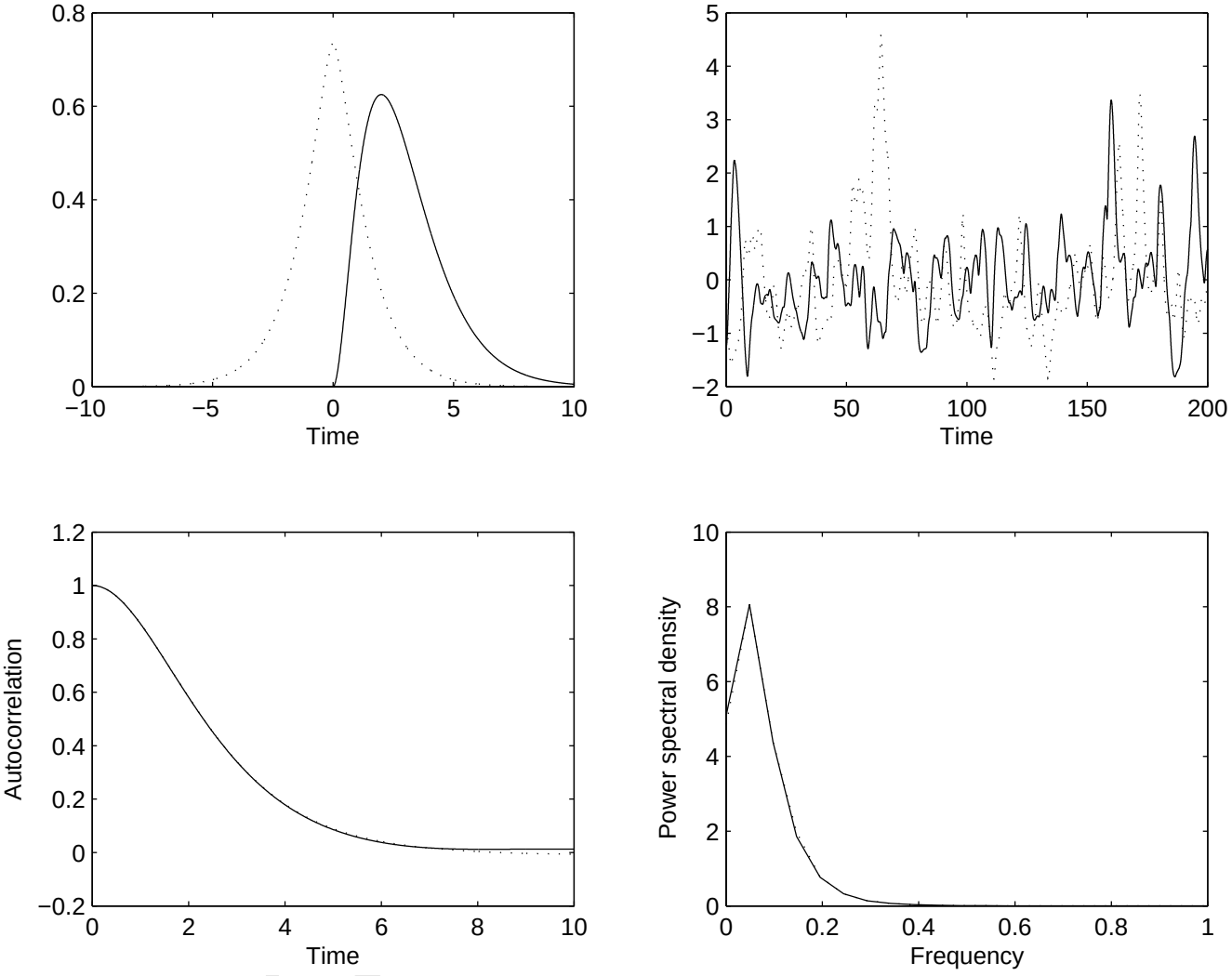

Figure 3: Example of $\mathcal{LMA}$. Top left: Kernel used; top right: Example of trajectories. Bottom left: Empirical autocorrelation function. Bottom right: Empirical power spectrum. For each plot: non-symmetric kernel f_1 in solid line and symmetric kernel case f_2 in dotted line. Parameters for the noise are $\lambda = 0,\ \psi = 1,\ \xi = 0.2,\ \zeta = 0.6$

comprehensive report on this subject. We use hereafter an estimate obtained by computing and averaging biperiodograms from overlapping blocks before applying a frequency-domain filter. This estimates of the bispectrum S_3 will be denoted $\hat{S}_3$. It is readily available in the HOSA toolbox for MATLAB.

In the case of X_t being a $\mathcal{LMA}$ process with underlying Laplace noise Γ and kernel f, its bispectrum can be expressed from the kernel using similar computations as in the case of the power spectrum. We obtain

$$S_3(\omega_1, \omega_2) = s(\Gamma) F(\omega_1) F(\omega_2) \overline{F(\omega_1 + \omega_2)} \tag{11}$$

where $s(\Gamma)$ is the third order moment of the Laplace noise Γ and $F = \mathcal{F}(f)$ the transfer function. In particular, one has the following relations, for any $\omega_1,\ \omega_2$:

$$|S_3(\omega_1, \omega_2)| = |s(\Gamma)||F(\omega_1)||F(\omega_2)||F(\omega_1 + \omega_2)|, \tag{12}$$

$$\Psi(\omega_1, \omega_2) = \Phi(\omega_1) + \Phi(\omega_2) - \Phi(\omega_1 + \omega_2), \tag{13}$$

where $\Psi(\omega_1, \omega_2)$ is the angle of $S_3(\omega_1, \omega_2)$ and $\Phi(\omega)$ is the angle of $F(\omega)$.

These relations show that unless the skewness of the noise is null, the kernel can be retrieved completely from the bispectrum. This will be used in the sequel to derive estimates for the kernel. In the case of null or very small skewness, the extension to fourth order could be necessary. It is straightforward in the mathematical formulation

$$S_4(\omega_1, \omega_2, \omega_3) = k(\Gamma) F(\omega_1) F(\omega_2) F(\omega_3) \overline{F(\omega_1 + \omega_2 + \omega_3)},$$

where $k(\Gamma)$ is the fourth order moment of the Laplace noise Γ. However, this approach will certainly meet numerical difficulties. The extension to the fourth order has not been studied in this work.

3. Fitting procedure

3.1. Kernel estimation

Up to now, only symmetric kernels have been estimated in the literature for $\mathcal{LMA}$ processes (see aforementioned references). However, we have seen in the previous section that a symmetric kernel is not able to retrieve front-back asymmetries existing in records. We will recall some particular cases of kernels, before introducing a new estimator.

3.1.1. Usual estimates

Assume we observe a sequence $(X_{t_1}, \ldots, X_{t_n})$ from a $\mathcal{LMA}$ with unknown parameters and kernel f. Let $\hat{S}$ be the empirical spectrum. Our goal is to a find an estimate $\hat{f}$ for the kernel that allows for asymmetries and respect the second order structure of the observed process. It means that we will impose that the spectrum (or autocorrelation) of the fitted process to be the same as the observed one. Thus the square magnitude of the Fourier transform of the kernel (or finite impulse response) will be held fixed to the observed spectrum, i.e. $|\mathcal{F}\hat{f}|^2 = \hat{S}$. From this relation, it is clear that we still have an infinite number of kernel with the same magnitude, if we allow the phase to change, and we build estimates $\hat{f}$ of the kernel f as following:

$$\mathcal{F}\{\hat{f}\}(\omega) = \sqrt{\hat{S}(\omega)}\, \exp\{i\hat{\Phi}(\omega)\}, \tag{14}$$

where $\hat{\Phi}$ is an unknown function. Three classical kernels in signal processing, which correspond to different general choices for $\hat{\Phi}$, are detailed bellow.

Symmetric kernel. This is the kernel used in reference studies. It is obtained by assuming $\hat{\Phi} = 0$. This is a non-causal kernel, symmetric with respect to the origin, but that cannot be adequate for modeling front-back asymmetries;

Anti-symmetric kernel. Assume the phase is $\hat{\Phi}(\omega) = -\operatorname{sgn}(\omega)\frac{\pi}{2}$. Then the kernel will be odd. It can be seen from eq. (6) that the resulting process will have a skewness of 0, and thus can not model marginal asymmetries. Moreover, it is shown in [12] that a $\mathcal{LMA}$ with an odd kernel can not generate any time irreversibility, and we thus decided to drop this model hereafter.

Minimum Phase kernel. The particular case of minimum phase kernel is obtained by setting $\hat{\Phi} = \mathcal{H}\{\log\sqrt{\hat{S}}\}$, where $\mathcal{H}$ is the Hilbert transform. In this model we have a direct relation between the magnitude and the phase via the Hilbert transform $\mathcal{H}$. This kernel is causal (null for negative lags), thus asymmetric, and allows for front-back asymmetries. This is the estimate obtained when fitting a stationary ARMA model, in a discrete-time context.

3.1.2. Spline estimator for the phase

None of the kernels presented above may be suited for the observed time series, because all of them rely on a strong assumption on the process that cannot be verified easily. In order to adjust the kernel to the records, a classical approach is to use the *bicepstral method*. In this method, a kernel estimate is obtained using the complex cepstrum, as described in [13, 10]. It thus relies on 2D Fourier transform to identify an arbitrary kernel, by inverting the relation (11). The obtained estimate for the kernel will be used as a reference. Instead of this approach, we propose here to estimate the phase of the transfer function with *regression splines*. Splines are piecewise polynomials smooth functions. They are defined by their knots, their degree, and the coefficients of the polynomials within each knot (see e.g. [14] and [15] and references therein for more details). The vector of coefficients will be denoted θ in the sequel.

We used this tool to estimate the phase Φ, by approximating this unknown function by a cubic spline function, $\Phi_s(\omega;\theta)$. The estimation of the coefficients of the regression spline can be performed by using the relation (13). More precisely, hereafter $\hat{\theta}$ is defined as

$$\hat{\theta} = \arg\min_{\theta} \sum_{i,j} |\hat{S}_3(\omega_i,\omega_j)|(1-\cos\left(\hat{\Psi}(\omega_i,\omega_j) - \Phi_s(\omega_i;\theta) - \Phi_s(\omega_j;\theta) + \Phi_s(\omega_i+\omega_j;\theta)\right), \qquad (15)$$

where $\hat{S}_3$ is the empirical bispectrum, estimated as described in Section 2.4. The distance $1-\cos(.)$ was used because the phase is unchanged when adding $2k\pi$ for any $k \in \mathbb{Z}$. The weights $\hat{S}_3(\omega_i,\omega_j)$ are added because the angle is badly estimated for very small values of the magnitude, and thus we reduce the importance of such observations. We used a numerical optimization algorithm to solve this problem. This obtained kernel is thus

$$f_{\text{spline}} = \mathcal{F}^{-1}\left\{\hat{S}(\omega)\exp\left[i\hat{\Phi}_s(\omega;\hat{\theta})\right]\right\} \qquad (16)$$

and will be referred as the 'spline kernel' in the sequel.

3.2. Parameters estimation

In this section we assume that the kernel is known. The aim is to estimate the four parameters of the underlying Laplace noise. Following [5], we will use a moment estimator based on the marginal

moments, expressed earlier (equations 2—5), meaning that we will replace the moments values in those equations by their empirical counterparts, and inverting the obtained system.

As described in [5] it can happen that this system has no solution, because the constraint in equation (6) may not be fulfilled by the empirical estimates of moments, due to the sample variability of these quantities or because the marginal distribution is not a $\mathcal{GAL}$. In this case, an approximate solution is chosen, and one can refer to [5] for the choice of the approximation. We will follow their choice in this study.

The consistency of the estimates can be derived from the strong mixing property of moving averages with respect to Lévy measures, as $\mathcal{LMA}$ are (see, for example [16]). This ensures that the empirical moments converge to the true values, leading to consistency.

4. Simulation results

In this section, we study the behavior of the estimates using simulations.
The procedure is the following, repeated 1000 times:

1. Simulate a $\mathcal{LMA}$ with known kernel (symmetric and minimum phase, see equations 8 and 8 and Figure 3);
2. Estimate the kernel assuming that it is a symmetric or minimum phase (see Section 3.1.1) or using the bispectral and splines methods (see Section 3.1.2);
3. For each kernel estimate, deduce estimate of the $\mathcal{GAL}$ parameters using the method introduced in Section 3.2 and do the same using the true kernel for comparison purpose;
4. Simulate a long realization of the fitted model to estimate its the dynamical characteristics.

According to Table 2, the symmetric, minimum phase and spline kernels lead to similar results both in terms of bias and variance as concerns the estimation of the marginal parameters. There is a systematic positive bias in estimating ξ while the parameter ζ is under-estimated. This may be due to the correlation between those two estimates (not shown here). The bicepstral method leads to rather different results, with a lower variance, but a higher bias for both parameters. The third column of Table 2, which contains the L^2 distance $\int (f(x) - \hat{f}(x))^2 dx$ between the true kernel f and the estimated one $\hat{f}$, suggests that it may be due to a bad estimation of the kernel. It implies that the system of equation (2—5) has more often no solution than with the other method (4.5% for this method, less than 1% for the others) and explains the higher bias in the estimates of the marginal parameters. Note that using the wrong assumption on the kernel (e.g. assuming that it is symmetric whereas the true process has a minimum phase kernel) lead to a bad estimation for the kernel. It is then interesting to observe that the spline model provides a good estimate in both cases, almost as good as when using the true model, with a slightly higher variance. When comparing with the kernel obtained by the bicepstral method, we see a great improvement. We also studied numerically the importance of the number of knots of the splines and their location, but found that those two parameters do not have a great influence on the results (not shown for the sake of conciseness). The latter remark only applies to this particular case for which the phase function is smooth enough. If this function has many peaks, a more advanced fitting procedure may be applied, following for example [17].

Figures 4 and 5 show the various kernel estimates. From these plots, it is clear that the spline model allows to recover the asymmetries in the kernel, by allowing the phase to be non-zero in the minimum phase case (right bottom plot, Figure 4), while for the symmetric kernel case, the

True process	Minimum phase kernel							
Parameter	ξ	ζ	L^2 error	A	$\delta_{\text{up}}^{\text{Crest}}$	$\delta_{\text{down}}^{\text{Crest}}$	$\delta_{\text{up}}^{\text{Trough}}$	$\delta_{\text{down}}^{\text{Trough}}$
Actual values	0.2	0.6	NA	-0.21	0.41	0.56	0.33	0.46
True Kernel	0.25 (0.08)	0.55 (0.12)	NA	-0.21 (0.07)	0.41 (0.01)	0.56 (0.03)	0.33 (0.01)	0.47 (0.03)
Symmetric kernel	0.25 (0.08)	0.55 (0.12)	0.50 (2.10)	0.00 (0.06)	0.57 (0.02)	0.57 (0.02)	0.34 (0.01)	0.34 (0.01)
Minimum phase kernel	0.25 (0.09)	0.56 (0.12)	0.00 (0.01)	-0.21 (0.07)	0.42 (0.01)	0.56 (0.02)	0.35 (0.01)	0.49 (0.02)
Bicepstral method	0.19 (0.06)	0.42 (0.09)	0.17 (1.12)	-0.33 (0.16)	0.89 (0.17)	3.02 (0.40)	0.69 (0.07)	1.30 (0.41)
Spline kernel	0.25 (0.08)	0.54 (0.12)	0.01 (0.03)	-0.16 (0.09)	0.44 (0.02)	0.57 (0.02)	0.33 (0.01)	0.42 (0.02)
True process	Symmetric kernel							
Parameter	ξ	ζ	L^2 error	A	$\delta_{\text{up}}^{\text{Crest}}$	$\delta_{\text{down}}^{\text{Crest}}$	$\delta_{\text{up}}^{\text{Trough}}$	$\delta_{\text{down}}^{\text{Trough}}$
Actual values	0.2	0.6	NA	0.00	0.55	0.55	0.33	0.33
True Kernel	0.23 (0.07)	0.56 (0.10)	NA	0.00 (0.07)	0.55 (0.02)	0.55 (0.02)	0.33 (0.01)	0.33 (0.01)
Symmetric kernel	0.24 (0.07)	0.56 (0.10)	0.00 (0.00)	0.00 (0.07)	0.57 (0.02)	0.57 (0.02)	0.33 (0.01)	0.33 (0.01)
Minimum phase kernel	0.24 (0.07)	0.63 (0.10)	0.48 (2.00)	-0.16 (0.08)	0.42 (0.01)	0.57 (0.03)	0.34 (0.01)	0.49 (0.02)
Bicepstral method	0.16 (0.05)	0.43 (0.08)	0.25 (1.38)	-0.26 (0.10)	1.08 (0.09)	3.49 (0.33)	0.82 (0.08)	1.34 (0.37)
Spline kernel	0.24 (0.07)	0.56 (0.10)	0.01 (0.01)	0.01 (0.08)	0.55 (0.02)	0.55 (0.02)	0.33 (0.01)	0.33 (0.01)

Table 2: Parameters estimation for two kernels (minimum phase and symmetric) and four estimation methods. In bracket, the standard deviation based on 1000 i.i.d replications.

obtained kernel is almost symmetric (right bottom plot, Figure 5). This is important in practical applications, since it might be interesting to recover the asymmetries in the records.

As stated in Section 2, one needs additional criteria than the parameters of the Laplace noise to fully describe the ability for the fitted process to recover the characteristics of the original data. Hence, we compared the asymmetry criteria introduced earlier. Results are given in the five rightmost columns of Table 2. It can be concluded from this table that the spline model allows to retrieve the shape of the 'waves' for the two type of processes considered here. This was not possible neither with the symmetric kernel nor the minimum phase kernel. We also found that the biceptrum method was not well suited, since the estimated value differ greatly from the true values. This is the reason why we did not use this estimator in the application part that follows.

5. Application to wave times series

In this section, the proposed methodology is illustrated on a time series of sea wave measured in a wave flume on a varying bottom, in the situation described in Figure 6. The wave flume is forced from the left with infinite-depth Gaussian waves, with a typical JONSWAP spectrum with $\gamma = 3.3$ (see e.g [18] Eq. 2.4.1), and waves propagate to the right and tends to shoal as the depth decrease. At a fixed location (point 8, situated at $X = 7m$), one obtains a time series of elevation of the free surface, presented in the upper-left corner of Figure 8. It can be seen from this plot that the data indeed exhibits differences between front and back slopes, revealing time-irreversibility (see the values in Table 3), and also discrepancies between crests and troughs (vertical asymmetry, refer to the positive value of the skewness).

Figure 7 shows the periodogram which is a usual estimate of the the power spectrum. In this plot, we see three main peaks which appear due to non-linear waves interactions, since an unimodal power spectrum is introduced in the wave flume. These non-linear interactions are even clearer when looking at the bisepctrum (upper-left plot of Figures 10 and 11) with peaks at coupled frequencies. We recall that for a Gaussian process, the bispectrum will be identically zero, and thus this assumption is not well suited here.

The marginal distribution of the observed sequence is too lightly tailed compared to a $\mathcal{GAL}$ distribution (see eq. 6). To deal with this problem, we transform the process so that its marginal distribution lie in the acceptable space for a $\mathcal{GAL}$ distribution, which is a quite usual way in time series modeling with e.g. the Box-Cox transformation. We chose the following arbitrary non-linear transform

$$Y = \begin{cases} \exp\left(|X|.^{1/2}\right) - 1 & \text{if} \quad X \geq 0 \\ -\exp\left(|X|.^{-1/2}\right) - 1 & \text{if} \quad X < 0 \end{cases} \tag{17}$$

which allows for higher asymmetry and heavier tails. It would be interesting to propose a more systematic procedure to chose such function. Descriptive statistics of this transformed process are given in the upper-left corner of Figures 8 to 10 and in the first line of Table 3.

$\mathcal{LMA}$ is fitted to this transformed time series using the different kernel (symmetric, minimum phase and spline) estimates. The kernels corresponding to each fitted model are shown in Figure 9. One can clearly see the differences between the kernels, in particular the spline estimated kernel, which is neither symmetric nor minimum phase and looks almost like a typical wave. As mentioned in the introduction, a particular impetus for this work was to develop stochastic models which can generate artificial but realistic waves. In this context, it seems natural to simulate long sequences of the fitted models (see Figure 8 for examples of simulated sequences) and compare the statistical

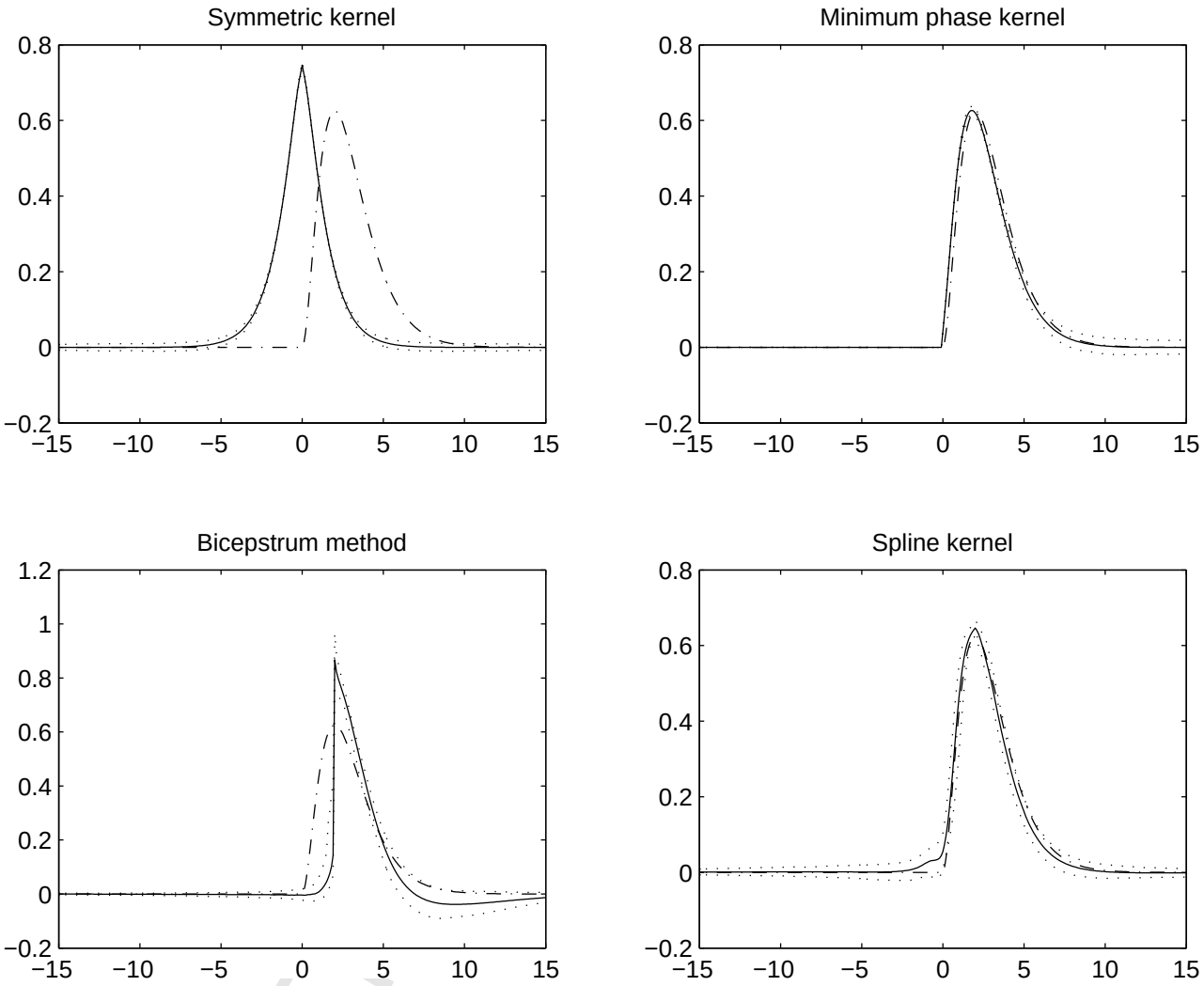

Figure 4: Estimation of the kernel for a minimum-phase process and three different estimates for the kernel. Dashed-dotted line: true kernel; solid line: mean estimated kernel; dotted line: 95% confidence interval based on 1000 i.i.d. replications.

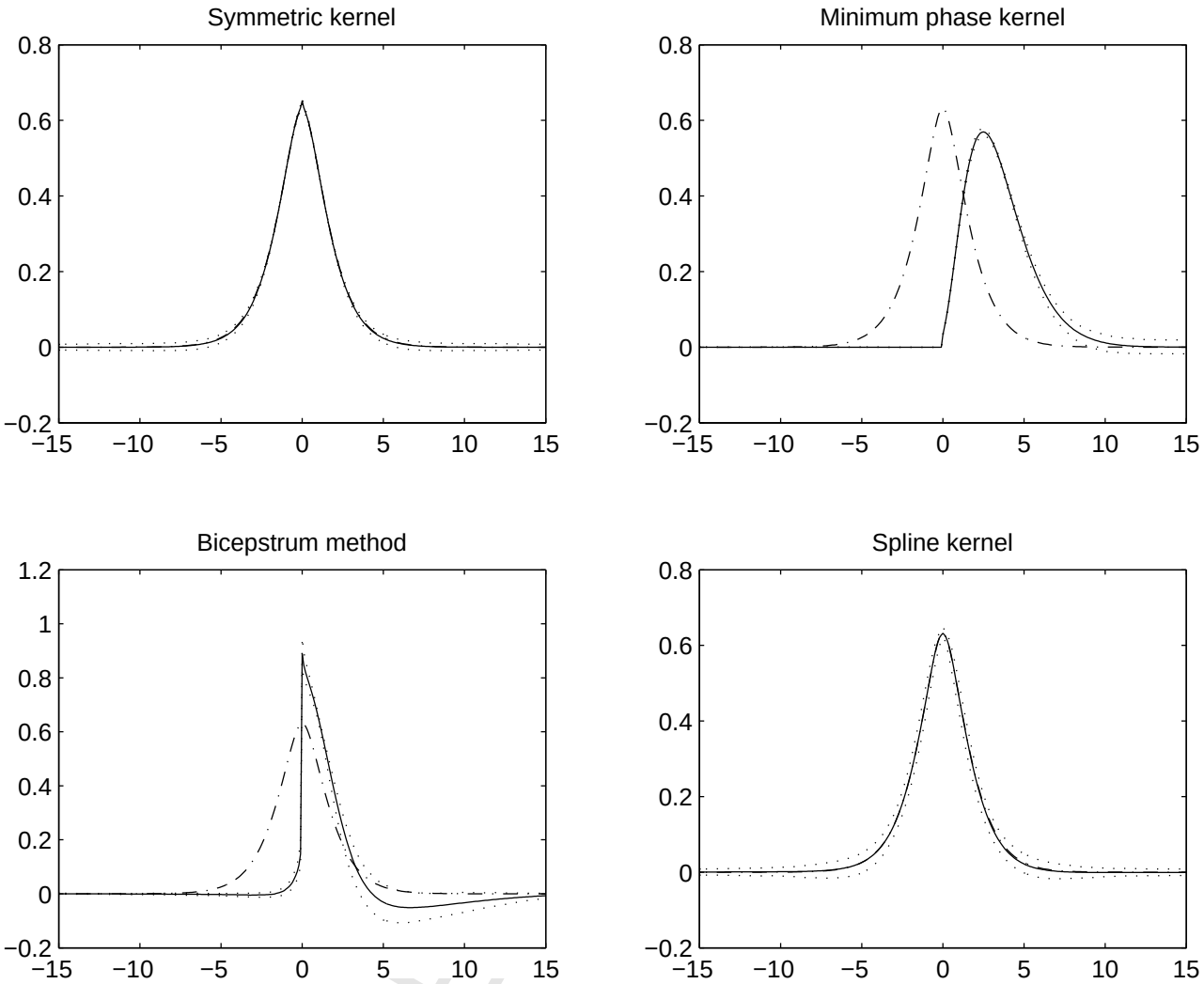

Figure 5: Estimation of the kernel for a symmetric process and three different estimates for the kernel. Dashed-dotted line: true kernel; solid line: mean estimated kernel; dotted line: 95% confidence interval based on 1000 i.i.d. replications.

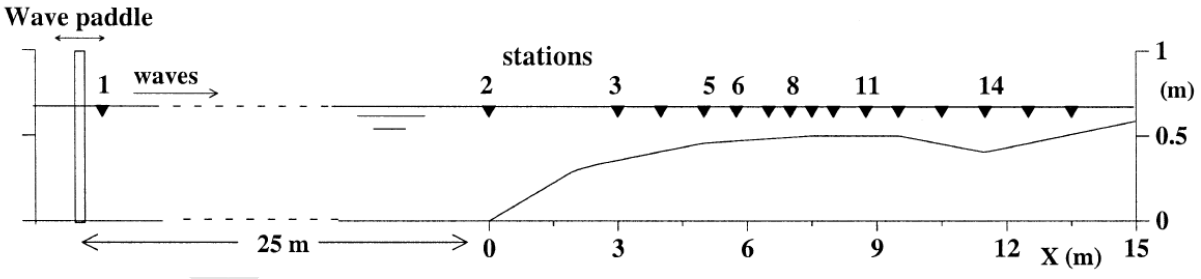

Figure 6: Experimental layout.

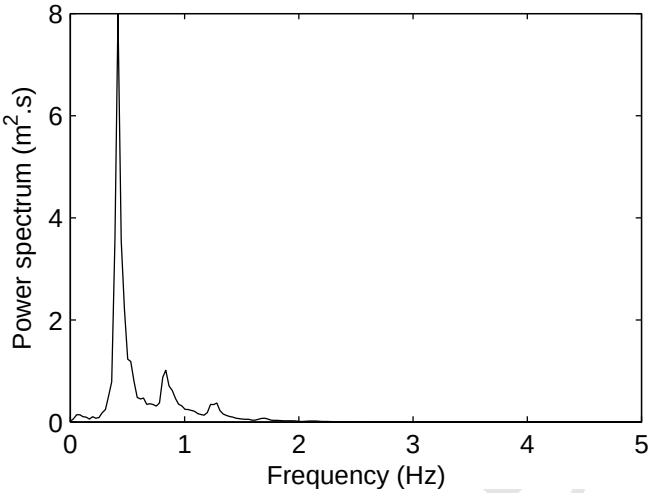

Figure 7: Power spectral density of observations.

properties of the artificial sequences with the ones of the original data. The variability of the various estimates has been estimated using parametric bootstrap (see e.g [19]). Note that it is difficult to compute a likelihood function of residuals for the fitted models and thus to use the standard statistical diagnostic tools used in time series analysis.

We first looked at the bispectrum in order to see if one can retrieve the coupling between components which symbolized by the non-zero values. The logarithm of the absolute value of each bispectrum is shown in Figure 10 whereas the angle of each bispectrum can be found in Figure 11. Both figures have been computed on the transformed time series to simplify the discussion. Figure 10 shows that globally, the shape of the bispectrum is well retrieved, much better than with a Gaussian process for which the bispectrum would be identically zero. However, we observe more low-frequency peaks on the bispectra of fitted models, and less peaks at high frequencies. This is probably due to the constraint imposed when using a linear process defined by (13). According to Figure 11, the spline kernel outperforms the other estimate and the shape of the phase of the bispectrum is well retrieved. As expected, the symmetric kernel has a zero phase, and the phase of the minimum phase model is rather complicated, but linked to the Hilbert transform of the spectral density of the process, and both of these are far from the observations.

Finally the fitted spline model allows to retrieve the first four moments of the process (see Table 3), the second order dependence structure and some characteristics of the bispectrum, much better than with the previously existing methods. We will now look at the tilting properties of the models, and compare them to the observed data, in the original scale, meaning that the fitted models are transformed back via the inverse of the marginal transform. Again, according to Table 3, the spline model globally outperforms the two other models as far as asymmetry criteria are concerned. Indeed, despite a small increase in the variance, all the values are closer to the true ones. In particular, the minimum-phase kernel, which also permits to retrieve asymmetries, fails to recover the good ratio between front and back slopes, both for crests and troughs. As said in previous sections, the symmetric kernel is unable to reproduce asymmetry in the records apart from vertical asymmetries. This is verified in Table 3 and confirms that this type of kernel lacks flexibility to model non-linear time series.

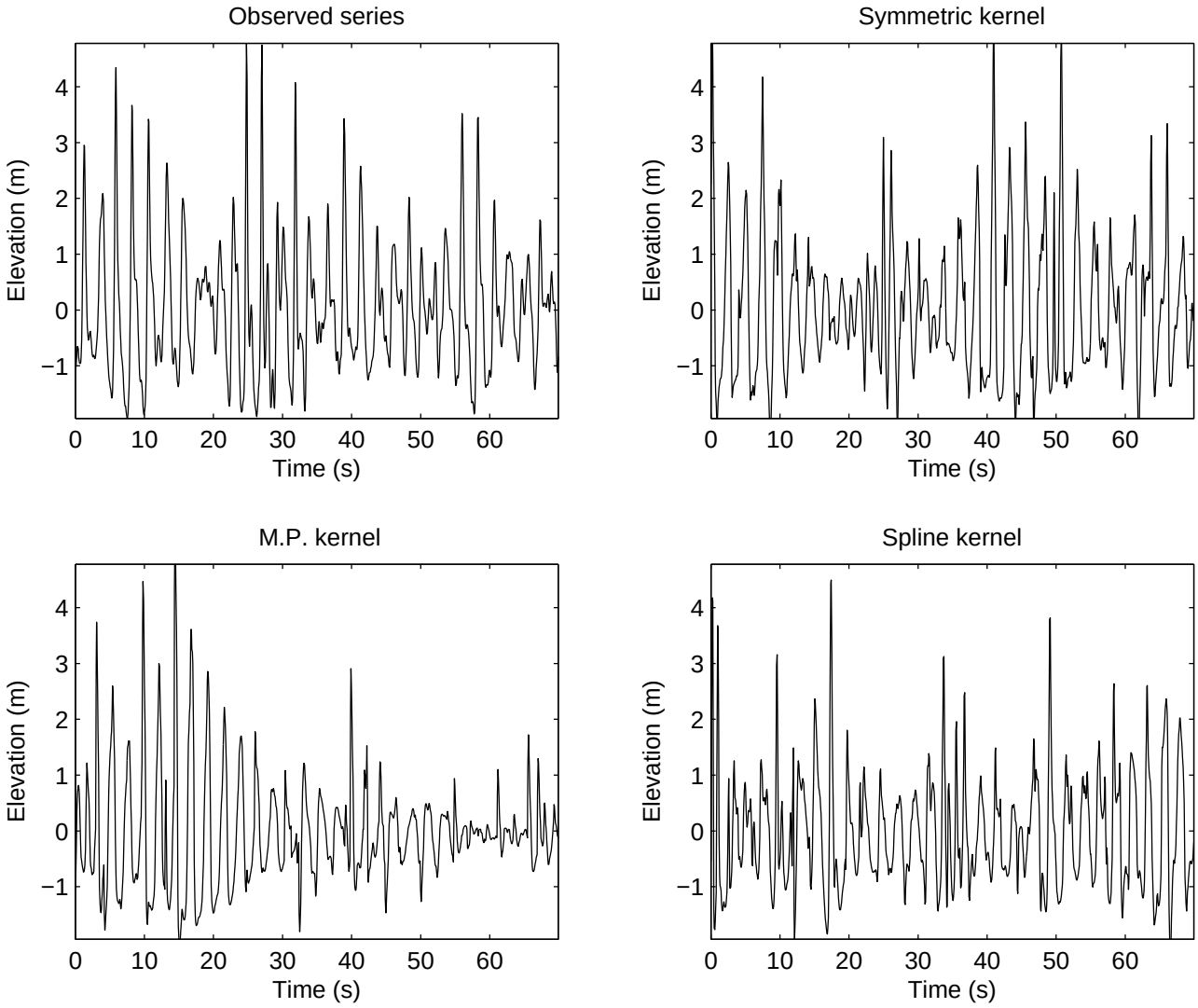

Figure 8: Example of sequences simulated with the fitted models.

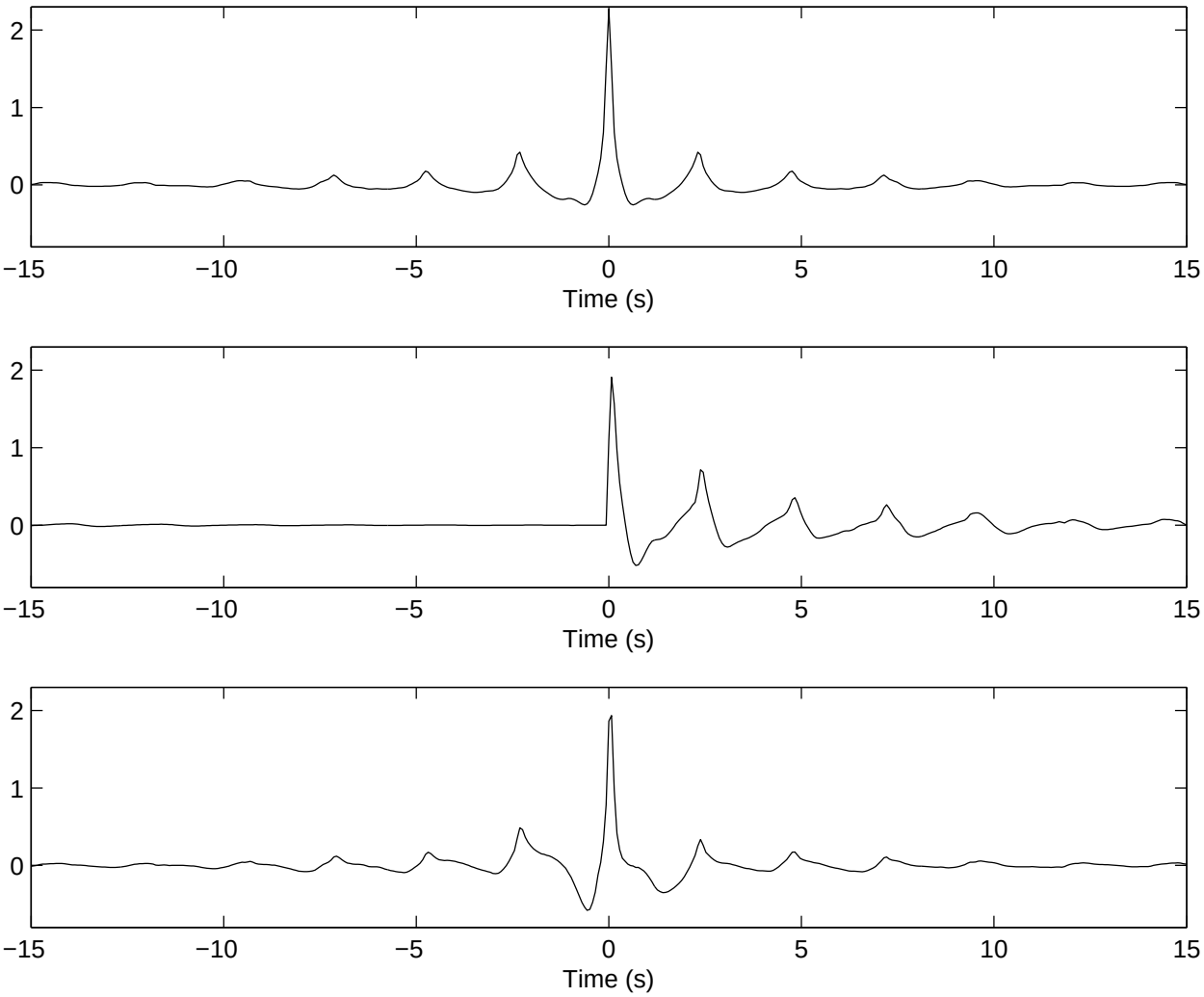

Figure 9: Estimated kernels. From top to bottom: symmetric model, minimum phase model, spline model.

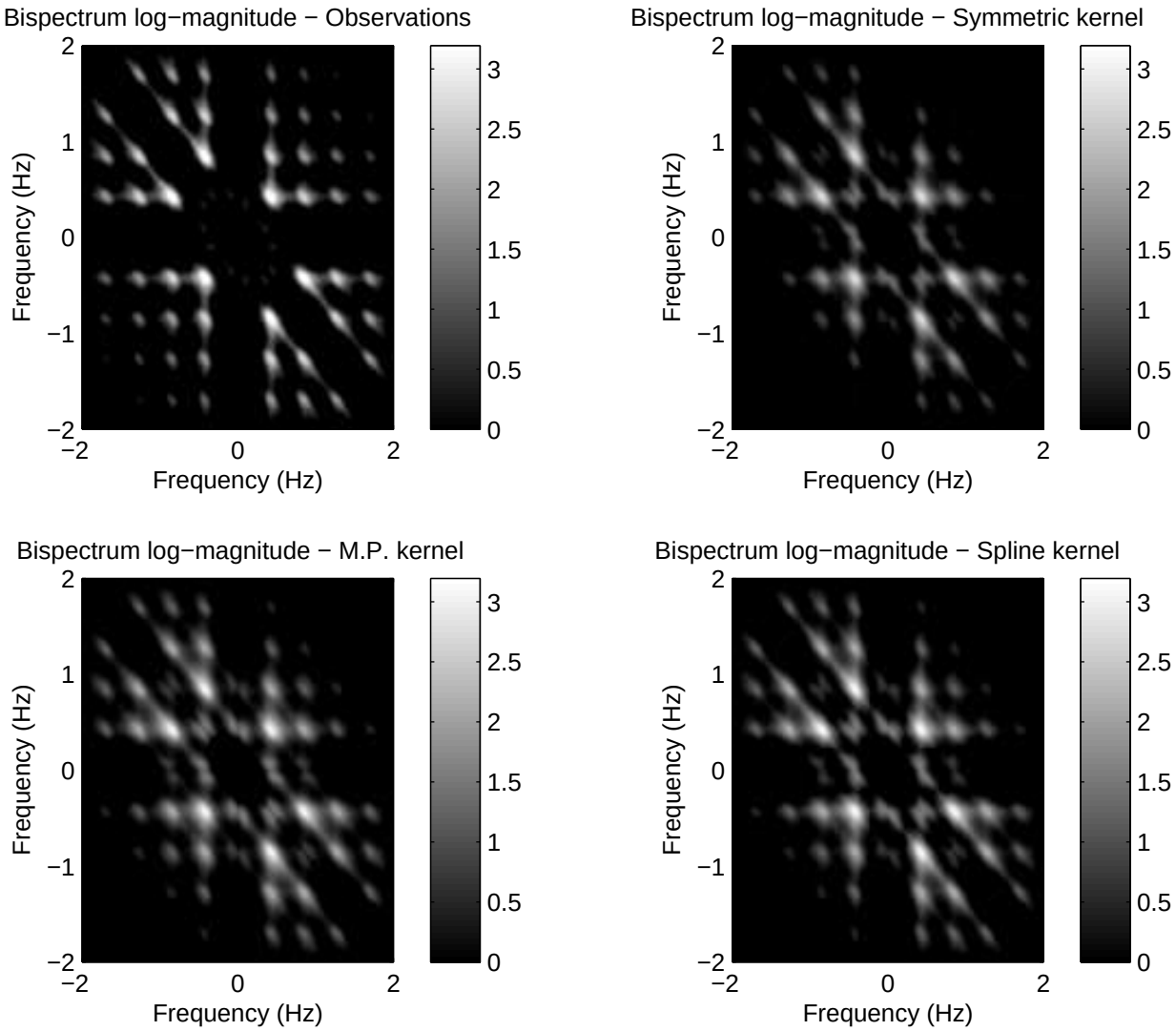

Figure 10: Log-magnitude of bispectra for the transformed process (top left) and the fitted models.

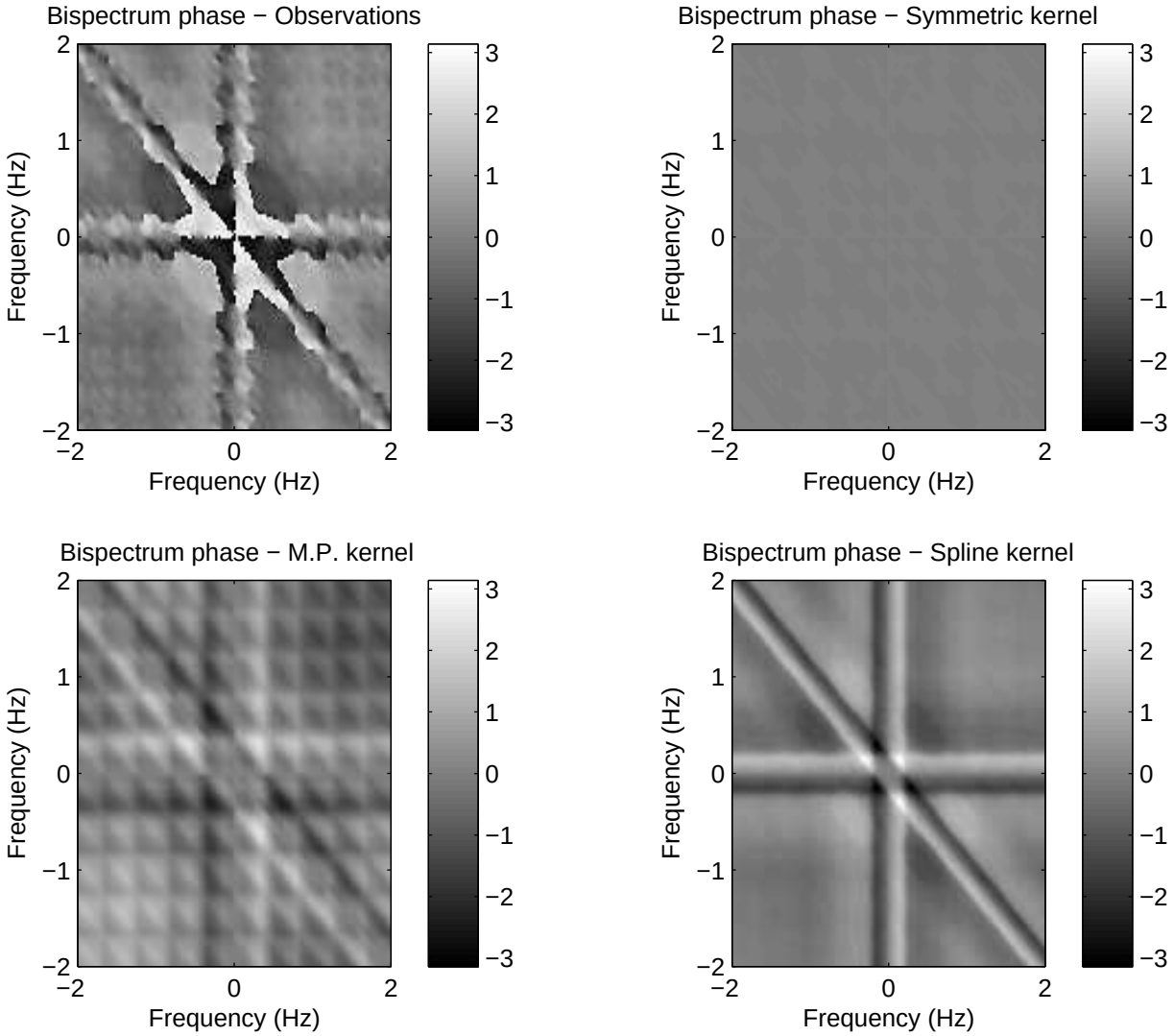

Figure 11: Angle of bispectra for the transformed process (top left) and the fitted models.

Parameter	Median	Skewness	Kurtosis	Asymmetry	$\delta_{\text{up}}^{\text{Crest}}$	$\delta_{\text{down}}^{\text{Crest}}$	$\delta_{\text{up}}^{\text{Trough}}$	$\delta_{\text{down}}^{\text{Trough}}$
Observations	-0.10	0.89	4.87	-0.63	3.88	5.29	2.03	2.82
Symmetric kernel	-0.15	1.08	5.29	0.00	5.10	5.12	3.07	3.08
	(0.04)	(0.10)	(0.65)	(0.01)	(0.28)	(0.29)	(0.16)	(0.16)
Minimum phase kernel	-0.11	1.04	5.25	0.37	4.42	4.90	3.44	2.81
	(0.04)	(0.10)	(0.80)	(0.07)	(0.24)	(0.39)	(0.17)	(0.20)
Spline estimated kernel	-0.10	0.97	5.07	-0.32	4.37	5.70	2.99	3.07
	(0.03)	(0.08)	(0.62)	(0.04)	(0.34)	(0.31)	(0.16)	(0.12)

Table 3: Dynamical criterion estimates for the three models, for the original data. In brackets, the standard deviation obtained via parametric bootstrap.

Even if the spline model is the closest one to the data, it still fails to reproduce the observed values. This might be due to constraints imposed when using linear filtering. To check this, we performed a linearity test based on the bicoherence (see [10] and the HOSA toolbox for Matlab) which rejected the linearity of the process, although each fitted LMA process pass the test. Hence, the discrepancies between the fitted model and the observed data may be linked to the choice of a too restrictive linear model.

6. Conclusion

In this article we proposed a method to model time series that exhibits both horizontal and vertical asymmetries. The model is based on a novel versatile tool, called $\mathcal{LMA}$, which involves four parameters for the marginal distribution and a function called kernel. A new estimator based on splines has been proposed to estimate this function. Thanks to an inclusive numerical study, the performances of the new model have been checked and it shows great improvement compared to the previous estimator available. Some future work is also left on the construction of a parametric model on the phase of the transfer function to ease the estimation procedure.

We also tested the proposed methodology on a time series of sea waves. We checked that both horizontal and vertical asymmetries are well respected, along with dynamical parameters such as the skewness of the Hilbert transform or the crests and troughs slopes. The procedure shows great enhancement compared to existing methods. However it still shows some discrepancies, that seems to come from the non-linearity of the data. Hence, some improvements are still needed to overcome this, for example by using a second-order model to enhance the model.

Acknowledgments

The authors gratefully acknowledge the financial support from national French ANR project MODNAT. We are also grateful to the reviewers for their constructive comments and suggestions, which have led to significant improvements to the paper.

References

1. Podgórski, K., Wegener, J.. Non-gaussian fields with vertical and horizontal asymmetries. *Preprint* 2010;.

2. Aberg, S., Podgórski, K.. A class of non-gaussian second order random fields. *Extremes* 2011;14:187–222. 10.1007/s10687-010-0119-1.

3. Galtier, T., Gupta, S., Rychlik, I.. Crossings of second-order response processes subjected to LMA loadings. *J Probab Stat* 2010;2010:22 pages. doi:10.1155/2010/752452.

4. Galtier, T.. Note on the estimation of crossing intensity for Laplace moving average. *Extremes* 2011;14:157–166.

5. Podgórski, K., Wegener, J.. Estimation for stochastic models driven by Laplace motion. *Communications in statistics Theory and methods* 2011;40:3281–3302.

6. Kotz, S., Kozubowski, T., Podgorski, K.. The Laplace Distribution and Generalizations: A Revisit With Applications to Communications, Exonomics, Engineering, and Finance. Progress in Mathematics Series; Birkhäuser Boston; 2001. ISBN 9780817641665.

7. Funke, E., Mansard, E.. The control of wave asymmetries in random waves. *Coastal Engineering Proceedings* 1982;1(18):725–744.

8. Masuda, A., Kuo, Y.Y.. A note on the imaginary part of bispectra. *Deep Sea Research A* 1981;28:213–222. doi:10.1016/0198-0149(81)90063-7.

9. Elgar, S.. Bispectra of shoaling ocean surface gravity waves. In: *Higher-Order Spectral Analysis, 1989. Workshop on*. 1989:206–211. doi:10.1109/HOSA.1989.748765.

10. Nikias, C., Petropulu, A.. Higher-order spectra analysis: a nonlinear signal processing framework. Prentice Hall signal processing series; PTR Prentice Hall; 1993. ISBN 9780136782100.

11. Rao, T.S., Gabr, M.. An introduction to bispectral analysis and bilinear time series models. Lecture Notes in Statistics, 24. New York etc.: Springer-Verlag. VIII, 280 p.; 1984.

12. Wegener, J.. Noise Convolution Models: Fluids in Stochastic Motion, Non-Gaussian Tempospatial Fields, and a Notion of Tilting. Doctoral theses in mathematical sciences; Faculty of Engineering, Centre for Mathematical Sciences, Mathematical Statistics, Lund University; 2010. ISBN 9789174730326.

13. Pan, R., Nikias, C.. The complex cepstrum of higher order cumulants and nonminimum phase system identification. *Acoustics, Speech and Signal Processing, IEEE Transactions on* 1988;36(2):186–205. doi:10.1109/29.1513.

14. Fan, J., Yao, Q.. Nonlinear Time Series: Nonparametric and Parametric Methods. Springer Series in Statistics; Springer; 2008. ISBN 9780387693958.

15. Hastie, T., Tibshirani, R., Friedman, J.. The elements of statistical learning. 2nd ed.; Springer; 2009.

16. Cambanis, S., Podgórski, K., Weron, A.. Chaotic behavior of infinitely divisible processes. *Studia Mathematica* 1995;115(2):109–127.

17. Spiriti, S., Eubank, R., Smith, P.W., Young, D.. Knot selection for least-squares and penalized splines. *Journal of Statistical Computation and Simulation* 2013;83(6):1020–1036.

18. Hasselmann, K., Barnett, T., Bouws, E., Carlson, H., Cartwright, D., Enke, K., Ewing, J., Gienapp, H., Hasselmann, D., Kruseman, P., et al. Measurements of wind-wave growth and swell decay during the Joint North Sea Wave Project (JONSWAP). Tech. Rep.; Deutches Hydrographisches Institut; 1973.

19. Benton, D., Krishnamoorthy, K.. Performance of the parametric bootstrap method in small sample interval estimates. *Advances and Applications in Statistics* 2002;2:269–285.